Available online at www.sciencedirect.com
SCIENCE DIRECT®
Journal of Structural Biology 144 (2003) 79–94
Journal of Structural Biology
www.elsevier.com/locate/yjsbi

Automated determination of parameters describing power spectra of micrograph images in electron microscopy

Zhong Huang, Philip R. Baldwin, Srinivas Mullapudi, and Pawel A. Penczek*

Department of Biochemistry and Molecular Biology, The University of Texas—Houston Medical School, 6431 Fannin, MSB 6.218, Houston, TX 77030, USA

Received 8 September 2003, and in revised form 13 October 2003

Abstract

The current theory of image formation in electron microscopy has been semi-quantitatively successful in describing data. The theory involves parameters due to the transfer function of the microscope (defocus, spherical aberration constant, and amplitude constant ratio) as well as parameters used to describe the background and attenuation of the signal. We present empirical evidence that at least one of the features of this model has not been well characterized. Namely the spectrum of the noise background is not accurately described by a Gaussian and associated "*B*-factor;" this becomes apparent when one studies high-quality far-from focus data. In order to have both our analysis and conclusions free from any innate bias, we have approached the questions by developing an automated fitting algorithm. The most important features of this routine, not currently found in the literature, are (i) a process for determining the cutoff for those frequencies below which observations and the currently adopted model are not in accord, (ii) a method for determining the resolution at which no more signal is expected to exist, and (iii) a parameter—with units of spatial frequency—that characterizes which frequencies mainly contribute to the signal. Whereas no general relation is seen to exist between either of these two quantities and the defocus, a simple empirical relationship approximately relates all three.

Keywords: Power spectrum; Electron microscopy

1. Introduction

Electron microscopy (EM)[1] plays an important role in molecular structural biology, as it enables observation of macromolecules in the close-to-native state. One immediately encounters several issues when one starts to process images with the goal of obtaining high-resolution 3-D maps. First, one must assess the quality of the micrographs from which particle images are selected in order to assess the number of particle images needed. During this data retrieving process, at least three experimental and instrumental factors need to be completely understood. The first is the contrast transfer function (CTF), which quantitatively describes the image distortions due to the defocus and spherical aberration of the electron microscope as a function of spatial frequency (Wade, 1992). The second is the effective envelope function (E), which represents attenuations due to several factors including the lack of spatial and temporal coherence as well as specimen motion (Wade, 1992). The third is the background noise (N) (Glaeser and Downing, 1992; Zhu et al., 1997).

A good estimation of image quality in terms of contrast above background depends on the estimation of the parameters in CTF, E, and N, which describe all the information included in a micrograph image except for the particle signal. Therefore, there is a need for a fully automated toolkit that allows the assessment of the quality of the micrographs, together with the calculation of the CTF parameters. From these assessments, moreover, the knowledge of the signal-to-noise ratio

* Corresponding author. Fax: 1-713-500-0652.
E-mail address: pawel.a.penczek@uth.tmc.edu (P.A. Penczek).

[1] *Abbreviations used*: EM, electron microscopy; 1-D, one-dimensional; 2-D, two-dimensional; 3-D, three-dimensional; 3-D EM, three-dimensional electron microscopy; CTF, contrast transfer function; CF, cut-off frequency; PPF, predominant power frequency.

1047-8477/$ - see front matter © 2003 Elsevier Inc. All rights reserved.
doi:10.1016/j.jsb.2003.10.011

(SNR) characteristics of the collected EM data may be utilized to properly align particle views and filter the resulting structure.

In practice, it is difficult to separate background noise from the particle signal. Empirically, the power spectrum of the background noise has been modeled as an exponential function of frequency. In this study, we develop a semi-empirical method to estimate the parameters in the CTF function as well as to find low-order polynomials demarcating $\log E$ and $\log N$ that take advantage of an inequality and equality constrained linear optimization fitting algorithm (Barrodale and Roberts, 1978, 1980).

As a byproduct, it is noted that there is no clear-cut relation between image quality, defocus and what has been increasingly called in the literature as the *B*-factor (Saad et al., 2001). Indeed, we have many examples to show that a single Gaussian function cannot possibly describe the asymptotic behavior of the power spectrum with respect to frequency. Instead of *B*-factor, we introduce two parameters with the units of spatial frequency (1/Å) to give an indication of micrograph quality. The foremost we call the cut-off frequency (CF), and it is defined as the spatial frequency at which we expect no more reliable signal (as measured by how well the purported signal correlates with CTF oscillations). The second quantity, the predominant power frequency (PPF) indicates which frequencies (the PPF and below) where the predominant part (99%) of the signal power is contained. If the CF and PPF are both high, we would intuitively call this a "good" micrograph, meaning that the bulk of the signal is at high frequencies. If the CF is high, but the PPF is low, the situation is cloudier as there is relatively small amount of signal at high frequency.

Recently two new methods for automated determination of CTF parameters have been published (Mindell and Grigorieff, 2003; Sander et al., 2003). In both methods, the defocus estimation is based on the cross-correlation between a generated CTF curve and the power spectrum after background subtraction. In the first method, the uncertainity of the background noise estimate is reduced by simply smoothing the original power spectrum (by a box convolution of Fourier amplitudes) but there is no use of envelopes in the defocus estimation. Moreover this estimation is performed using data in the entire frequency regime, which can have a large (and adverse) effect on the calculated parameters. The second method is mainly geared towards classification of power spectra using principal component analysis. The overall goal is a more precise assignment of defocus values to the individual particle images. Still, the frequency region where the CTF effect is to be studied must ultimately be defined by the user. In addition, there is a single *B*-factor used to characterize the envelope function in the defocus estimation, which is not the proper representation of the decay of the power spectrum, as we will show in this work. Our method remains distinct from these works with respect to the following aspects: (i) the elimination of the low-frequency signal which is not useful for parameter estimation, and (ii) how to obtain a proper envelope function for the defocus estimation. We will give more detailed comparisons in Section 2.

The manuscript is organized as follows. In Section 2, we introduce a method for separating the particle spectrum from the background noise and for estimation of the astigmatism. In Section 3, we describe how to fit the CTF parameters to the data. Because one of the theses of this manuscript is that the *B*-factor does not characterize micrographs very well, we develop expressions for two quantities to be used in its stead: the cut-off frequency (CF) and the principal power frequency (PPF). In Section 4, we simulate data with values of the parameters described above and show that these parameters can be recovered. Next, we use our method to determine parameters for micrographs collected under a wide variety of microscopy conditions: strong versus weak CTF effect, carbon support versus no carbon. We also show that our procedures are effective no matter how the power spectrum of the micrograph is estimated. Plots demonstrating each stage of the analysis are given. Additional tests are performed on the set of experimental micrographs and the results of the automated, manual, and self-consistent estimates of defocus values are given. We demonstrate that an empirical relationship seems to approximately linearly unite the three crudest frequency-dependent characteristics of a micrograph: CF, PPF, and 1/defocus. Section 5 contains discussion and conclusions.

2. Methodology

2.1. Linear model of image formation in the electron microscope

If we assume that both the transfer and the envelope functions are spatially invariant and that the noise is additive and uncorrelated with the signal, then the image formation process in EM is described by

$$o(x,y) = \mathrm{ctf}(x,y) \otimes e(x,y) \otimes s(x,y) + n(x,y), \tag{1}$$

whose Fourier space version is

$$O(\omega_x,\omega_y) = \mathrm{CTF}(\omega_x,\omega_y)E(\omega_x,\omega_y)S(\omega_x,\omega_y) + N(\omega_x,\omega_y). \tag{2}$$

Here o is the observed image, s is the imaged object, $\otimes$ is the convolution operator, n is the noise, ctf is the point spread function and e is the inverse Fourier transform of the envelope function E. Also, the independent variables ω_x and ω_y are spatial frequencies, and CTF is the

contrast transfer function. Finally S, N, and O are the Fourier transforms of s, n, and o, respectively. It is often convenient to express Eq. (2) in polar coordinates:

$$O(\omega,\theta) = \mathrm{CTF}(\omega,\theta)E(\omega,\theta)S(\omega,\theta) + N(\omega,\theta), \tag{3}$$

where $\omega = \sqrt{\omega_x^2 + \omega_y^2}$ is the magnitude of the spatial frequency and $\theta = arctg(\omega_y/\omega_x)$. In the absence of directional distortions and astigmatism, the envelope and transfer functions are rotationally symmetric and depend on ω, but not θ, so that the Eq. (3) can be further simplified.

In the weak-phase approximation, the contrast transfer function of the electron microscope is given by Wade (1992):

$$\mathrm{CTF}(\omega,\theta) = \sin\left(\gamma(\omega,\theta) - arctg\left(\frac{Q}{1-Q}\right)\right), \tag{4}$$

where $0 \leqslant Q < 1$ is the amplitude constant ratio, γ is the phase shift defined by

$$\gamma(\omega,\theta) = 2\pi\left(-\frac{C_s\lambda^3\omega^4}{4} + \frac{\Delta z'(\theta)\lambda\omega^2}{2}\right), \tag{5}$$

where C_s is the spherical aberration constant, λ is the electron wavelength, and $\Delta z'$ is the defocus (a positive value corresponds to an under-focus) and depends on the amplitude A_a and the angle A_θ of astigmatism via

$$\Delta z'(\theta) = \Delta z + \frac{A_a}{2}\sin(2(\theta - A_\theta)). \tag{6}$$

Here Δz is the average defocus or the defocus in the absence of astigmatism. If there is no astigmatism ($A_a = 0$), the transfer function (Eq. (4)) is independent of the angle θ. Astigmatism ($A_a > 0$) results in the elliptical elongation of the transfer function in the direction $\theta = A_\theta + \pi/4$.

A number of envelope functions have been introduced to account for effects such as partial coherence, finite source size (Frank, 1973), energy spread (Wade and Frank, 1977), drift, specimen charging effect, multiple inelastic–elastic scattering (Kenney et al., 1992), and resolution-limiting influence of the photographic film used to collect the data (Downing and Grano, 1982). In practice, however, it has become common to replace the product of these envelopes by a simple, effective envelope function. This envelope function can have either the form of a polynomial (Zhou and Chiu, 1993) or can be more simply selected to be a one-parameter Gaussian function (Saad et al., 2001; Zhu et al., 1997):

$$E(\omega) = \mathrm{e}^{-2B\omega^2}. \tag{7}$$

The effective envelope function, E, of Saad and coworkers that appears in Eq. (7) describes the decay of Fourier amplitudes of the specimen signal (it is actually the square of the E that appears in Eq. (2)). Incidentally Eq. (7) has the same form as the temperature factor used in X-ray crystallography to characterize the influence of the thermal vibrations of atoms in crystals on structure factors (Drenth, 1999), so—per analogy—the constant in Eq. (7) is referred to as B-factor. Nevertheless, it has to be remembered that the factor B in Eq. (7) does not have any simple physical interpretation.

The power spectrum is defined as an expectation value of the Fourier intensities of the observed image. Assuming that the noise in Eq. (3) is uncorrelated with the signal, we obtain:

$$PW(\omega,\theta) = \langle O^2(\omega,\theta)\rangle = \mathrm{CTF}^2(\omega,\theta)E^2(\omega,\theta)S^2(\omega,\theta) + \tilde{\sigma}_N^2(\omega,\theta), \tag{8}$$

where $\tilde{\sigma}_N^2$ is the power spectrum (i.e., the Fourier space variance) of the background noise N and $\langle\bullet\rangle$ denotes the expectation value.

We define a one-dimensional (1-D) power spectrum that is rotationally averaged in the angular range θ_1 to θ_2 as:

$$P_{\mathrm{rot}}(\omega) = \frac{1}{(\theta_2 - \theta_1)}\int_{\theta_1}^{\theta_2} PW(\omega,\theta)\,\mathrm{d}\theta. \tag{9}$$

In the absence of astigmatism, the 1-D power spectrum provides a robust estimate of the CTF effects on the image; therefore, it is often used in initial steps of the retrieval of the CTF parameters.

2.2. Estimation of the power spectrum

A robust estimation of the power spectrum is an important first step in the analysis of CTF effects. The two most commonly used approaches take advantage of the large amount of the available data and use averaging of micrograph sections to reduce noise. The first step involves the calculation of periodograms of micrograph sections. A periodogram is defined as the squared amplitude of the discrete Fourier transform of the image. It can be shown that a periodogram is an asymptotically unbiased estimate of the true power spectrum. That is, with the increased windowed length, the periodogram values approach the true power spectrum values. Unfortunately, a periodogram is not a consistent estimate of the power spectrum, as its variance does not decrease with the increased windowed length. In fact, the variance of the periodogram is of the same order as the variance of the estimated power spectrum (Kumaresan, 1993). Therefore, Welch (Welch, 1967) suggested sacrificing the resolution of the estimation for the decrease in variance and average periodograms of windowed segments of the data. Additional reduction of the variance is achieved by allowing the segments to overlap.

In electron microscopy, the averaging of periodograms is applied in two contexts. In the first approach (Fernandez et al., 1997; Zhu et al., 1997), Welch's

method is applied to periodograms calculated for large overlapping (usually by 50%) segments of micrographs. The segments are usually much larger than the size of the imaged specimen and no provisions are taken to distinguish between the areas containing particles or simply the background. Since the segments are large, the resolution of the power spectrum estimate is sufficient to obtain a highly accurate value of the defocus. The method works particularly well if the specimen is prepared on carbon support; the latter is a source of strong noise that easily yields a distinguishable, characteristic imprint of the CTF in the power spectrum. However, since the selected segments contain a mixture of particles and background, the remaining parameters of the CTF (particularly the background and the envelope) cannot be easily interpreted in terms of the image formation model given by Eq. (1).

Saad and co-workers proposed an alternative approach, also based on averaging of periodograms (Saad et al., 2001). In their method, in order to relate the calculated power spectrum directly to the image formation model Eq. (1), the periodograms are calculated for segments containing (and with the size closely matching) individual particles. While the interpretation of the obtained power spectrum is easier, the accurate estimation of the CTF parameters is more difficult. The power spectrum calculated using windowed particles tends to be noisy, as the segment size has to be small. It is also worthwhile noting that in Saad's approach, the particle-picking step precedes the CTF estimation step. A future direction might be to use the CTF estimation to help pick particles, which the approach that we have earlier outlined would allow one to do (Huang and Penczek, submitted).

2.3. Estimation of CTF parameters

According to the accepted model of the image formation, the estimated power spectrum is a sum of two components (see Eq. (8)): the background noise and the product of the three quantities, S^2, CTF^2, and E^2, which result from the particles of interest. Therefore, the proper estimation of the CTF parameters depends strongly on the estimation of the background noise characteristics. The choice of the analytical form of the background function is somewhat arbitrary, as there are various sources of the background noise. The most prominent sources include statistical variation in the number of electron events that formed the observed image, inherent noise of the photographic film due to grain non-uniformity, and quantum noise of elastic and inelastic scattering.

Possible empirical choices for the background noise include a Gaussian function used by Zhu et al. (1997):

$$\tilde{N}_1^2(\omega) = c_1 + c_2 \exp\{[-(\omega/c_3)^2]\}, \tag{10}$$

where c_{1-3} are heuristic parameters to be determined. This is done by first locating the minima of the 1-D power spectrum and, second, by fitting a Gaussian curve (Eq. (10)) to their positions by adjusting parameters c_{1-3}. Finally, the defocus is estimated based on the assumption that the located minima of the power spectrum correspond to zeros of the CTF. The difficulty is in proper identification of the minima of the power spectrum. If any of the minima is missed or misindentified (particularly the first one), the resulting defocus values will be entirely incorrect. This is why this approach was never used in a fully automated mode. In addition, the presence of the envelope function is a source of additional systematic errors, as it shifts the positions of the minima of the power spectrum.

Saad and co-workers used a more complicated exponential function that contains four heuristic parameters (Saad et al., 2001):

$$\tilde{N}_2^2(\omega) = C_1 \exp\{C_2\omega + C_3\omega^2 + C_4\sqrt{\omega}\}. \tag{11}$$

In this approach, the 1-D power spectrum of the micrograph is also calculated as a first step and it is followed by a semi-automated estimation of the four parameters C_{1-4} (Saad et al., 2001). Next, the rotationally averaged Fourier amplitudes of the structure ($S(\omega)$ of Eq. (3)) are obtained from X-ray scattering experiments and are used to determine—in addition to the noise background and the CTF parameters—the signal-to-noise ratio in the data in a self-consistent procedure.

There have also recently appeared two additional approaches for CTF parameter estimation (Mindell and Grigorieff, 2003; Sander et al., 2003). Both methods (as well as our own) adopt a cross-correlation strategy between background-subtracted S^2 and CTF^2 E^2 to estimate the defocus. In the first method the authors used a box-convoluted power spectrum to approximate the background noise, but did not use an envelope in the defocus estimation (Mindell and Grigorieff, 2003). They then try to examine the effect of the CTF throughout the entire frequency regime, which will result in two difficulties. First, power spectra that have peaks at very low frequencies will give rise to an over-estimation of the defocus. Second, when one bases the defocus estimation directly on the cross-correlation between the background-subtracted power spectrum and the generated CTF curves, the defocus winds up being systematically overestimated. In the low defocus cases, this over-estimation can be large, to the point of making the rest of the calculations irrelevant.

Sander and co-workers used a two parameter Gaussian noise profile and a single B-factor envelope (Sander et al., 2003). Their CTF parameter estimation is iterative, and complicated. The definition of the region where the CTF is fitted needs to be determined by the user, and is only vaguely defined. They report, in our

approach the region of the spectrum for which parameters are calculated is clearly defined and determined automatically. The method yields excellent results (Section 4) for the envelope (the dotted line in Fig. 3A) the background (dashed line in Fig. 3B) functions, and also for the values for the astigmatism and defocus.

3. Automated estimation of the defocus and astigmatism

3.1. Introduction

The proposed automated method of determining CTF parameters retrieval is semi-empirical. Although we take advantage of the theoretical form of the CTF function, we use empirical forms for the background and envelope functions. In this respect, parts of the procedure are based on empirical observations made from electron microscopy data rather than theoretical justifications.

We begin with the estimation of the 2-D power spectrum of a micrograph (or a section thereof). We use Welch's method of averaged periodograms and assume that Eq. (2) holds, i.e., that the measured power spectrum of signal minus power spectrum of the background is linearly related to the power spectrum of the signal from particles. The initial estimate of the CTF parameters is done using 1-D rotational average of the power spectrum. The 1-D power spectrum profile has improved signal-to-noise ratio compared to the actual 2-D power spectrum; moreover, it is easier to fit 1-D functions. To estimate the defocus and astigmatism, we first need to remove the Fourier space variance of the background noise (termed background henceforth) from the power spectrum and obtain envelope functions. We use an inequality and equality constrained linear optimization method (Barrodale and Roberts, 1980) to fit the 1-D overall envelope and background curves to the 1-D power spectrum. Next, the analytical form of the CTF^2 is fitted and the defocus value is established. Based on the CTF parameters calculated for the 1-D power spectrum, analysis of the 2-D power spectrum is performed and the astigmatism parameters are calculated.

3.2. Analysis of the 1-D rotationally averaged power spectrum

The main goal of the analysis of the 1-D power spectrum is the determination of the defocus value. This is done by first fitting the empirical forms of the envelope of the 1-D power spectrum and the background curves and, second, by fitting the analytical form of the squared CTF multiplied by the estimated squared envelope curve to the background subtracted 1-D power spectrum. We assume that the 1-D power spectrum can be divided into two regions (Fig. 1):

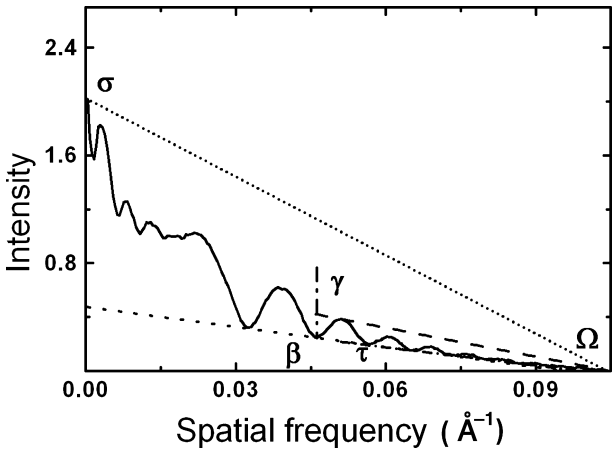

Fig. 1. In a procedure that isolates that part of the power spectrum from which one may determine parameters, one proceeds to find four points (σ, β, γ, and τ). First we indicate the largest frequency of the problem and denote it as Ω. We next find a line segment that is possibly close to the curve, over the entire frequency range, but yet remains above it. Such a line (short dotted line) will necessarily be tangent to the power spectrum curve at a point we call σ. Now on the interval determined by σ and Ω, we repeat the procedure and find a line segment that brackets the power spectrum from below: this is the dash dot line, which passes through the point β. This point divides the frequencies into two regions: high and low. Yet again we repeat this procedure, first from above (dashed line) yielding a point γ, and once more from below (dash dotted line) yielding a point τ. This yields the four points: σ, β, γ, and τ. The point γ will belong to a polynomial curve that is used to fit the high-frequency region of the power spectrum from above, whereas the point τ will belong to a polynomial curve that is used to fit the high-frequency region of the power spectrum from below. The text of Section 3.2 gives further details on how these polynomials are constructed, and the defocus thereafter estimated.

Region 1: Low frequency: the information in this region may be distorted by the unevenness of the micrograph (illumination, ice thickness, and such). Moreover it is not clear that the data in this region adheres to the model of image formation. This region is excluded from the defocus estimation.

Region 2: Intermediate and high frequencies: there are pronounced CTF effects within this region. This is the region for which the parameters are estimated.

The reason we doubt that the data in region 1 is adequately described by the image formation model is that it would seem that the Fourier intensities at low frequencies (after deconvoluting the affect of the CTF) would be far too large.

Unlike in earlier procedures (Zhu et al., 1997), instead of using positions of the minima of the power spectrum, we seek the solution to the problem of fitting a curve that lies under (or above) a given set of k experimental points, i.e., in our case the sampled rotationally averaged 1-D power spectrum. We seek therefore two functions: f^a that lies above the power spectrum and f^b that lies below. Since the power spectrum is a non-negative function, we restrict the power spectrum

bracketing functions (f^a and f^b) to the class of functions that are an exponentiation of a polynomial of the ηth degree:

$$f^{b(a)}(\omega) = \exp(-g^{b(a)}(\omega)). \tag{12}$$

with $g^{b(a)}(\omega) = \sum_{l=0}^{\eta} a_l \omega^l$. In addition, we introduce:

$$P_{\text{rot}}^{\log}(\omega) = \log(P_{\text{rot}}(\omega)). \tag{13}$$

In order to fit two curves that bracket the 1-D power spectrum, one proceeds by minimizing the target function

$$\min_{\{a_l\}} \sum_{i=1}^{k} \left| g^{b(a)}(\omega_i) - P_{\text{rot}}^{\log}(\omega_i) \right| \tag{14}$$

subject to the constraints

$$g^{b(a)}(\omega_i) - P_{\text{rot}}^{\log}(\omega_i) \leqslant (\geqslant) 0, \quad i = 1, \ldots, k. \tag{15}$$

Actually, since we divide the power spectrum into two regions with presumably different spectral characteristics, we assume that both the envelope and the background functions are different in the respective regions. We restrict ourselves now to the case of the intermediate and high frequencies, where we can interpret the CTF effects.

In order to solve the system given by Eqs. (14) and (15) we use the inequality and equality constrained linear optimization method, which is based on a modified simplex algorithm of linear programming, the so-called L_1 solution (Barrodale and Roberts, 1978). The simplex method is a conventional method of solving an overdetermined system of equations with constraints (Chong and Zak, 1996). The modified simplex method employs a more advanced search algorithm that reduces the total number of iteration steps and speeds up the optimization process (Barrodale and Roberts, 1978). It is preferable to minimize the L_1 norm (Eq. (14)) instead of the L_2 norm, as the former is generally less biased by the presence of large errors in the data. Although the current state of the art is to employ dual simplex algorithms (for a good review see Bixby, 2002), the simplex method we have described is sufficient for our only moderately difficult problem.

From the solution, we construct

$$E^2(\omega_i) = f^a(\omega_i) - f^b(\omega_i), \quad i = 1, \ldots, k, \tag{16}$$

$$U^2(\omega_i) = P_{\text{rot}}(\omega_i) - f^b(\omega_i), \quad i = 1, \ldots, k, \tag{17}$$

where $i = 1, \ldots, k$ label the points in the intermediate frequency region. Interpreted in terms of the image formation model Eqs. (2) and (8), f^b is the power spectrum of the background noise N, E is the envelope function, while U^2 is the product of the squared envelope E^2, the squared transfer function CTF^2, and the squared particle signal S^2.

The decomposition of the 1-D power spectrum according to Eqs. (16) and (17) makes it possible to estimate the defocus value. We ignore any influence of the particle signal on the product U^2. We also ignore, at this juncture, the possible influence of the astigmatism. We choose to maximize the correlation coefficient between the analytical CTF^2 multiplied by the estimated squared envelope and the 1-D power spectrum evaluated within the intermediate frequency region:

$$\Delta z' = \max_{\delta z} \frac{\sum_{\omega_l \leqslant \omega_i \leqslant \omega_m} \text{CTF}^2(\omega_i, \delta z) E^2(\omega_i) U^2(\omega_i)}{\sigma_{C^2} \sigma_{U^2}}, \tag{18}$$

where

$$\begin{aligned} \sigma_{C^2}^2 &= \sum_{\omega_l \leqslant \omega_i \leqslant \omega_m} \text{CTF}^4(\omega_i, \delta z) E^4(\omega_i), \\ \sigma_{U^2}^2 &= \sum_{\omega_l \leqslant \omega_i \leqslant \omega_m} U^4(\omega_i), \end{aligned} \tag{19}$$

and δz is the defocus varied within the physically permissible range.

In order to determine the polynomial degree, we use a simple heuristic strategy. We first detect the border points between the two power spectrum regions. This is done by fitting degree one polynomials bracketing $P_{\text{rot}}^{\log}(\omega)$ from above and below (Eqs. (14) and (15)). The point β in Fig. 1, where the polynomial bounding $P_{\text{rot}}^{\log}(\omega)$ from below is tangent to $P_{\text{rot}}^{\log}(\omega)$, is taken as the border point between the two frequency regions. Next, the fitting of polynomials of degree one is repeated, this time using samples of $P_{\text{rot}}^{\log}(\omega)$ for the frequencies given by β and higher. This yields two points, γ and τ (see Fig. 1). These latter two points are now used to calculate new bracketing polynomials and, using Eqs. (16)–(19), the corresponding defocus values. The calculations are done for polynomials with degree varying from one to six. Since the defocus estimation is very sensitive to the polynomial degree used for bracketing, we choose the polynomial degree equal to the number of zeroes of the CTF (within the analyzed region of the power spectrum) minus one. We do not examine polynomials of higher degree; otherwise, the bracketing curves would have spurious maxima and would result in a poor estimate of the defocus. In order to refine the initial estimate of the defocus, we use this estimate to locate the CTF zeros and the CTF peaks and repeat the procedure described above. We repeat the procedure outlined above by fitting the envelope from the first CTF peak and fitting the background from first CTF zero (that is, instead of γ, we use the first CTF peak; instead of τ, we use the first CTF zero).

3.3. Estimation of the astigmatism

In the presence of astigmatism, the 2-D CTF is no longer rotationally symmetric. Instead, it becomes elliptically elongated and the defocus becomes dependent on the angle θ (see Eq. 8). More precisely, the defocus is a sine

function of the angle, while the phase of the sine function defines the direction of the maximum defocus. Therefore, provided the defocus values can be estimated with sufficient accuracy for a number of angular directions, the necessary astigmatism parameters can be found by fitting the sine function to the calculated defocus points. In our procedure, we divide the 2-D power spectrum into a small number of L sectors, each sector spanning the angle

$$\zeta = \pi/L. \tag{20}$$

In practice, we set the number of sectors to ten. (In the presence of very strong astigmatism, we can set it to as many as 60, as we do in the numerical simulation of astigmatism.) Within each sector, we perform the rotational averaging

$$p_l(\omega) = \frac{1}{\zeta}\int_{(l-1)\zeta}^{l\zeta} p(\omega,\theta)\,\mathrm{d}\theta, \quad l = 1,\ldots,L, \tag{21}$$

and, assuming that the angle ζ is sufficiently small so that the defocus value within each sector is approximately constant, we estimate the defocus value using the strategy described in Section 3.2. The only modification involves the selection of the low-frequency cut-off point and the polynomial degrees. Since the overall defocus was already approximately estimated, it can be used as a reference in order to control defocus values found for individual sectors. Thus, initially we estimate the defocus values $\Delta\bar{z}_l, l = 1,\ldots,L$ for all angular directions $(l-0.5)\varsigma$ and in each case we use the same polynomial degree that was established for the overall power spectrum. Next, we adjust the polynomial degree for each sector independently:

$$\eta_l = \max\left[1, \mathrm{int}\left(\overline{\eta}\frac{\Delta\bar{z}_l}{\Delta\bar{z}}\right)\right], \quad l = 1,\ldots,L, \tag{22}$$

where $\overline{\eta}$ is the polynomial degree determined for the overall power spectrum, $\Delta\bar{z}$ is the corresponding overall defocus value, and $\Delta\bar{z}_l$ is the defocus corresponding to angular directions $(l-0.5)\varsigma$ calculated using polynomial degree $\overline{\eta}$. Finally, using the adjusted polynomial degrees η_l, we repeat the calculations for the defocus. Based on these values, we estimate both the angle A_θ and the amplitude A_a of the astigmatism using the following equations:

$$\Delta\tilde{z} = \frac{1}{L}\sum_{l=1}^{L}\Delta z_l, \tag{23}$$

$$a = \sum_{l=1}^{L}\Delta z_l \sin(2(l-0.5)\varsigma), \tag{24}$$

$$b = \sum_{l=1}^{L}\Delta z_l \cos(2(l-0.5)\varsigma), \tag{25}$$

$$A_a = \sqrt{a^2+b^2}, \tag{26}$$

$$A_\theta = \arctan(b/a) - \frac{\pi}{2}, \tag{27}$$

where $\Delta\tilde{z}$ is the final defocus estimate without the astigmatism. When performing the analysis of each sector, we use the first CTF zero as given by the determined defocus to demarcate the lower endpoint of the frequency region for which parameters are calculated.

3.4. Estimation of the frequencies characterizing micrographs: CF and PPF

Intuitively, we sense that the data from micrographs is no longer reliable when the power spectrum no longer contains the oscillations that we expect to find due to the CTF. We therefore introduce a dedicated measure to ascertain a high-frequency cutoff. We consider each interval with endpoints given by successive CTF zeros, and ask how well the power spectrum correlates with a product of CTF^2 and E^2 within that interval:

$$Q = \frac{\int\sqrt{P}\times\mathrm{CTF}\times E}{\sqrt{\int P}\sqrt{\int \mathrm{CTF}^2\times E^2}}. \tag{28}$$

Here the integration interval extends over the interval with CTF zeros as endpoints. The quantity Q is necessarily less than 1 due to the Cauchy–Schwartz inequality; empirically 0.8 is a good value to use as a cutoff. Therefore, we find the last of the intervals where $Q > 0.8$, and locate the unique CTF maximum within that interval. The frequency corresponding to this CTF maximum, we call the high-frequency cutoff (CF).

Now consider the parameter, B, of the so-called B-factor (Glaeser and Downing, 1992). It is found by fitting a Gaussian function to the envelope (formed as in Eq. (16) from the difference in the bracketing envelopes). Were it the case that the envelope were well described by a single Gaussian, then B would indicate not only (i) the limiting resolution, but also (ii) where the principal part of the power spectrum resided. However, empirically, we find that the shapes of the difference curves are often not well approximated by a single Gaussian. Moreover, there is seemingly no correlation between B and CF which we have just described above. And if we do insist on some systematic method for singling out a "best Gaussian", then B-factors do not turn out to be a reliable characterization of micrographs.

We have already introduced CF to handle one of the two meanings that one might have hoped to associate with B, namely (i) the limiting resolution. We next introduce a second parameter to handle the second meaning (ii). We term PPF, the predominant power frequency, to be the frequency below which 99% of the integrated power spectrum of the single particle (i.e., the power spectrum after background subtraction) resides. We shall see that the two quantities, CF and PPF,

together do indeed form a useful characterization of the micrograph.

4. Results

In the following five subsections we demonstrate the efficacy of our method. In the first four of these subsections we show that the automated fitting routines work efficiently, (i) whether or not there is astigmatism, (ii) no matter what the value of the defocus (within physically plausible limits), (iii) regardless of whether carbon support is used as support for the preparation of grids, and (iv) regardless of the way that the sections of micrograph are windowed. Throughout these first four subsections, we compare our estimates with manual estimates. To acquire manual estimates, we generate CTF and adjust the defocus so that the zero points agree with minima of the 1-D power spectrum of the micrographs. Finally, in the fifth subsection we demonstrate that the two new quantities that we introduce, PPF and CF, form a useful characterization of micrograph quality. Throughout this section, in addition to simulated data, we used four sets of micrographs collected with various microscopes and under different imaging conditions (Table 1).

4.1. Testing our method for determining the astigmatism using simulated data

In the current practice of EM, the micrographs that are selected for further analysis generally have weak astigmatism, with the astigmatism amplitude less than 1% of the defocus (Frank et al., 2000). Although we are able to estimate the astigmatism in such cases, generally we can neglect the affect of such astigmatism in further processing. Therefore, our tests are performed on simulated micrographs with strong astigmatism and we create estimates for the astigmatism angle, amplitude, and corrected defocus.

To this end, we generated simulated images with a variety of focal settings. Specifically, we stepped the defocus from a near defocus setting of 0.7 μm to a far defocus setting of 2.1 μm in steps of 0.2 μm, and estimated A_θ, A_a, and $\Delta\tilde{z}$ using the automated method we have already described. We first generate a fictitious "signal" by using a Gaussian noise with standard deviation 0.8 (in arbitrary units). Then we represent the background by generating an additional noise that has standard deviation 0.5. We next low-pass filter this "signal" and "noise" that we have just created: the filter radius is 0.39 for the "signal" and 0.29 for the "background" (in normalized frequency units). Then the transfer function is applied to the "signal". Finally we add the "background" to the "signal" to create the simulated micrographs. The image size used was 4096×4096 pixels, the pixel size was 4 Å, spherical aberration constant $C_s = 2$ mm, amplitude constant ratio $Q = 0.1$, the voltage $= 400$ kV, astigmatism angle 90 degrees, and with the astigmatism magnitude, A_a, equal to the defocus, Δz. We found that the cross-correlation of the estimated values of A_θ, A_a, and $\Delta\tilde{z}$ with the true values was unity indicating that our procedure works very well. Moreover, in Figs. 2A and B we show the nearly identical 2-D power spectra created from simulated and re-generated images, after automated estimation of the defocus and the astigmatism. In general, the automated method gives better estimations of A_θ, A_a, and $\Delta\tilde{z}$ for the far defocus micrographs than for near defocus micrographs, particularly in the presence of very strong astigmatism, since in the former case the CTF effect is stronger (see Section 4.3).

4.2. Defocus estimations (near and far defocus cases)

We have successfully applied our method to micrographs with far defocus settings and near defocus settings. Although it is generally quite easy to estimate defoci in the far defocus case, it can be quite difficult in the near defocus case.

In Fig. 3 we demonstrate the overall process of envelope and background fitting of a far from focus power spectrum. From the first CTF peak, both the fitted overall envelope and the background touch possible CTF peaks and zeros (Fig. 3A). There are hardly any spurious signal peaks (i.e., peaks which are not due to the CTF) that can be observed from the first CTF peak to higher frequencies. Our generated CTF multiplied by

Table 1
Four micrograph data sets used in tests of the automated CTF determination procedure: 70S ribosome (Malhotra et al., 1998), 40S ribosome (Spahn et al., 2001), KLH—keyhole limpet hemocyanin (Zhu et al., 2003), and GroEl (Ludtke et al., 2001)

Image conditions	Imaged specimen			
	70S	40S	KLH	GroEl
Voltage (kV)	100	200	120	350
Pixel size (Å)	4.78	2.8	2.2	2.8
Spherical aberration (mm)	2.0	2.0	2.6	4.1
Carbon support	Yes	Yes	No	No
Number of tested micrographs	18	13	162	5
Range of automatically estimated defocus (μm)	0.34–2.51	1.91–5.29	0.73–2.89	0.94–2.40

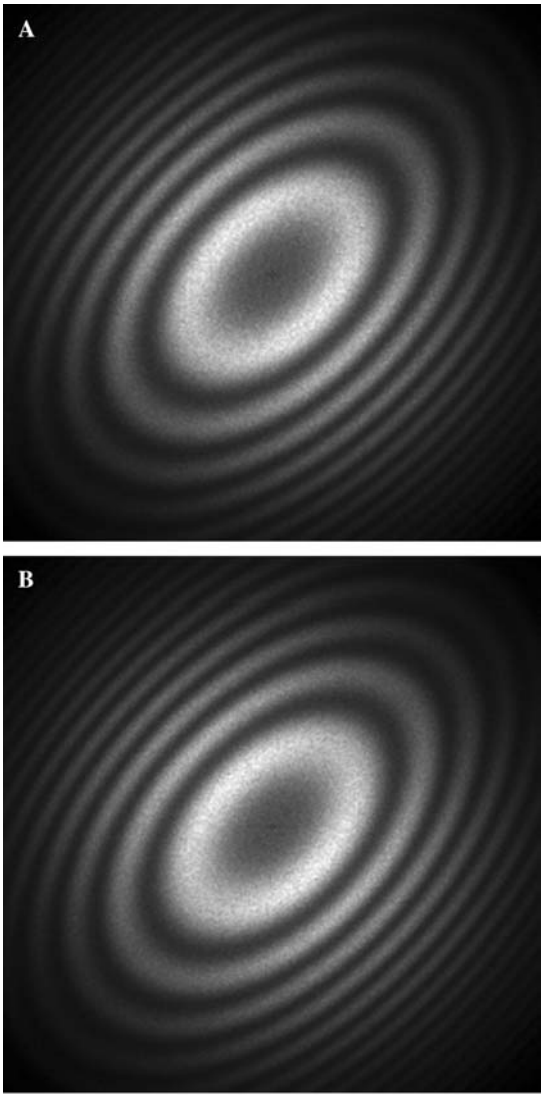

Fig. 2. Automated defocus estimation in the presence of strong astigmatism. We compare the 2-D power spectra of both the simulated micrograph and re-generated micrograph using estimated defocus, astigmatism angle, and amplitude. The determination of the astigmatism angle is described in the text. The simulated image condition is pixel size = 4 Å, spherical aberration constant $C_s = 2$ mm, amplitude constant ratio $Q = 0.1$, and the assumed microscope voltage is 400 kV. (A) 2-D power spectrum of a simulated micrograph with defocus 2.30 μm, astigmatism angle of 90°, and astigmatism amplitude 2.30 μm. (B) 2-D power spectrum of re-generated micrograph with automatically estimated defocus 2.29 μm, astigmatism angle 90°, and astigmatism magnitude 2.29 μm.

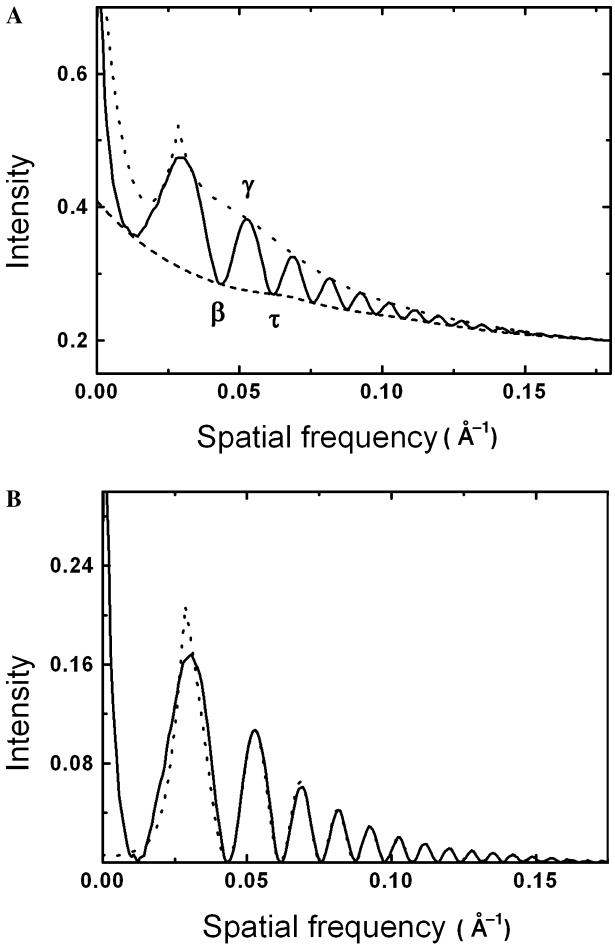

Fig. 3. The automated defocus estimation for far-from-focus 40S micrograph. (A) The power spectrum (solid), the overall envelope (dotted line), and the background (short dash line). (B) The signal (solid line), which is the power spectrum minus the background (both as shown in (A)). The curve given by CTF^2 E^2 (dashed line) is fit to the signal by selecting the defocus via Eq. (18). The estimated defocus is 2.07 μm, whereas the manually estimated defocus is 2.08 μm.

the squared envelope matches well with the background subtracted power spectrum (Fig. 3B). In general, the far defocus case is easier to process, because the power spectrum has easily discernible CTF peaks. The defocus estimation also agrees well with the manually estimated value.

In Fig. 4 we demonstrate how our method works in the very close to focus cases, where the 1-D power spectrum may have only a single peak attributed to CTF effects. The automatically estimated defoci (Figs. 4A, C and B, D) are very close in two tested cases: 0.43 and 0.47 μm, respectively. Because there is only one discernible power spectrum maximum, we were unable to estimate manual defocus values for these micrographs with a satisfying degree of accuracy. Notice in Fig. 4C that the second micrograph would appear to be more further from focus than the first micrograph (Fig. 4A), because the power spectrum at highest spatial frequency of 10 Å^{-1} has risen slightly more than for the power spectrum in first micrograph. That is, 10 Å^{-1} is further away from the last CTF zero in the second micrograph, indicating that the micrograph is further from focus. This heuristic argument substantiates what our method indicates about the defoci: they are close, but the second value is slightly larger than the first.

It is worth noting how crucial the selection of the background is to parameter estimation in the near defocus case. Improper selection of the background would

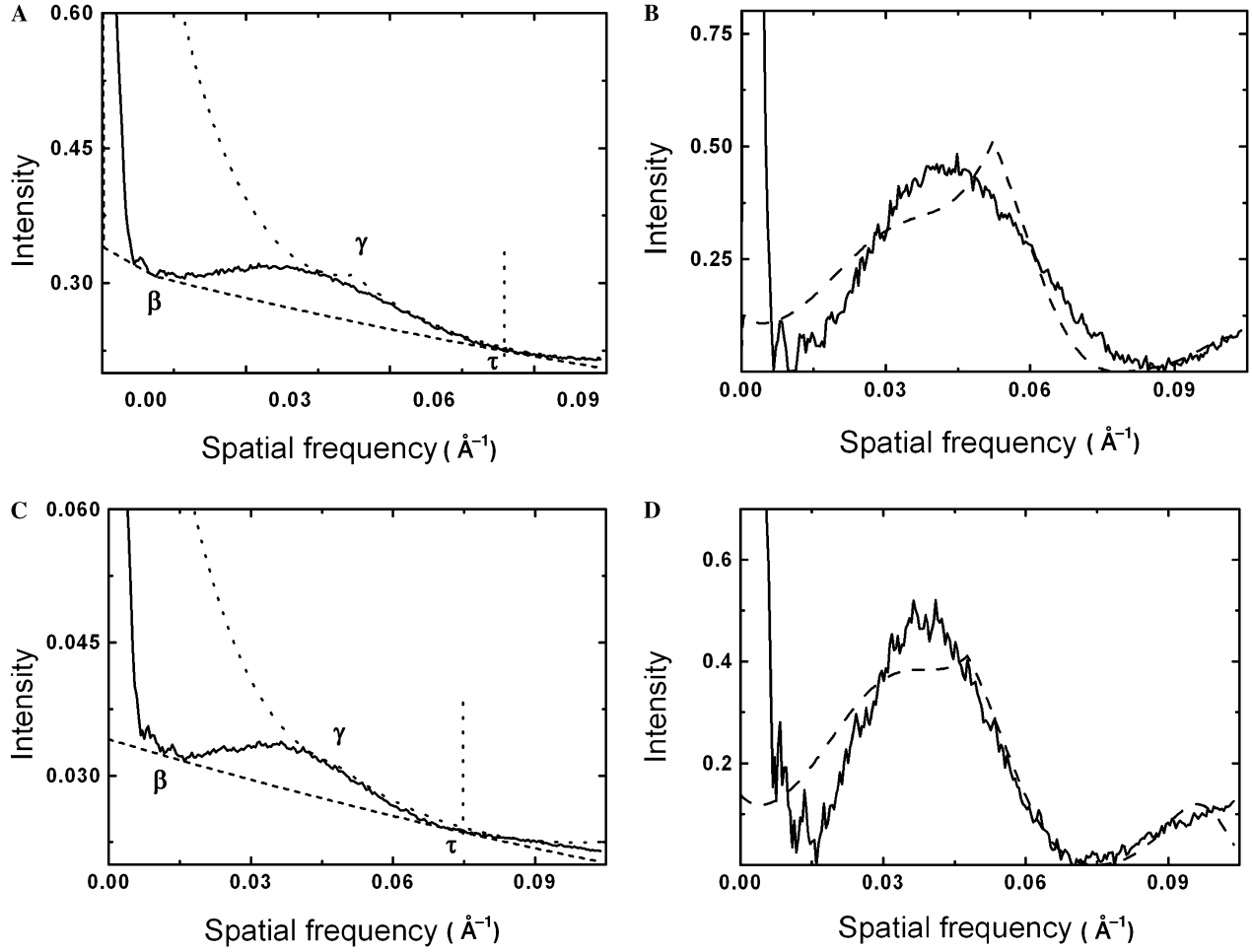

Fig. 4. The automated defocus estimation for near-to-focus 70S micrographs. (A) Power spectrum (solid line), envelope (dotted line), background (short dashed line). (B) Signal (solid line), and the curve CTF^2 E^2 (dashed line) using the estimated defocus. (C,D) Curves as in A, B that are derived from a second micrograph. The estimated defoci are 0.43 and 0.47 μm. That the second defocus is slightly larger is consistent with the shape of the curve at higher frequencies (see the text).

incorrectly emphasize small CTF peaks in the power spectra and typically lead to an overestimated defocus. The correct selection of the background allows us to differentiate two defoci that are very close.

4.3. Defocus estimation based on micrographs with a weak CTF effect

The examples of the last subsection were obtained using micrographs obtained with grids prepared with carbon support. However, we can perform successful estimations using micrographs that were obtained with grids without carbon support, and which therefore show a weak CTF effect, as is the case with GroEl data (see Table 1). This illustrated in Fig. 5, where an effect of the CTF on the power spectrum is very small, in comparison with Figs. 3A and 4A. In Fig. 5B we demonstrate that the method successfully ignores the irrelevant peaks at low frequencies, and gives a proper estimation of the defocus. The defocus estimated by this method gives 0.94 μm, which is close to 0.96 μm, is the value obtained by manual estimation.

4.4. Defocus estimation based on power spectra calculated from windowed particles, windowed sections of background noise, and overlapping sections of micrograph

As discussed in Section 2.2, there are two ways to obtain power spectrum. Normally, power spectra obtained in the way of (Saad et al., 2001) have high peaks (Fig. 6A) in the low-frequency region, due to the presence of strong particle signal. In these cases it becomes difficult to estimate the defocus if the low-frequency region is not handled well.

As a test of the effectiveness of our parameter estimation method, we estimated the defocus using different calculation strategies, and compared them. Specifically, we applied the strategy of (Saad et al., 2001) to calculate the power spectrum of windowed sections of background noise for the defocus estimation. We used the same

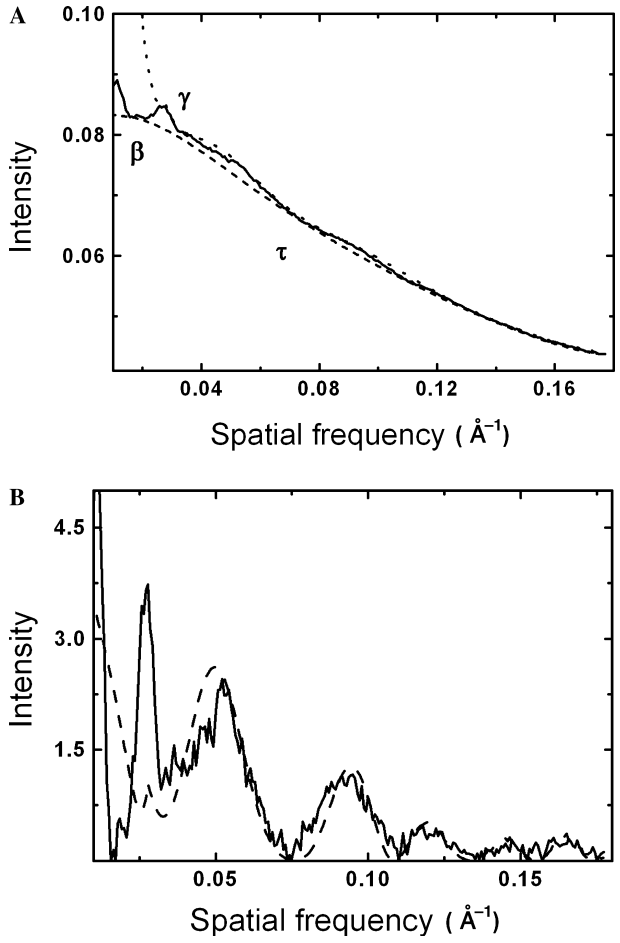

Fig. 5. The automated defocus estimation a GroEl micrograph exhibiting weak CTF effects. (A) Power spectrum (solid line), envelope (dotted line), background (short dashed line), signal (solid line). (B) Curve CTF^2 E^2 (dashed line) obtained using the estimated defocus. The estimated defocus is 0.94 μm, whereas the manually estimated defocus is 0.96 μm.

window size as in the case of windowed particles. Overall, this would seem a good strategy, since there are fewer irrelevant peaks in the low-frequency region (Fig. 6B), as compared to the same regions in power spectra obtained with the other two strategies (Figs. 6A and C).

In (Figs. 7A–C) we show comparisons of generated CTF (multiplied by envelope) curves with power spectra after background subtraction. The defoci obtained by the three different strategies (windowed particles, windowed noise and overlapping sections) were 2.49, 2.51, and 2.47 μm, respectively, while the manual estimation gave defoci of 2.43, 2.50, and 2.48 μm. Our method of estimating defocus, therefore, is successful regardless of how the power spectrum is calculated.

4.5. Verification of the accuracy of the automated defocus estimation method using experimental micrographs

In the absence of an external standard it is difficult to assess the accuracy of an automated defocus estimation

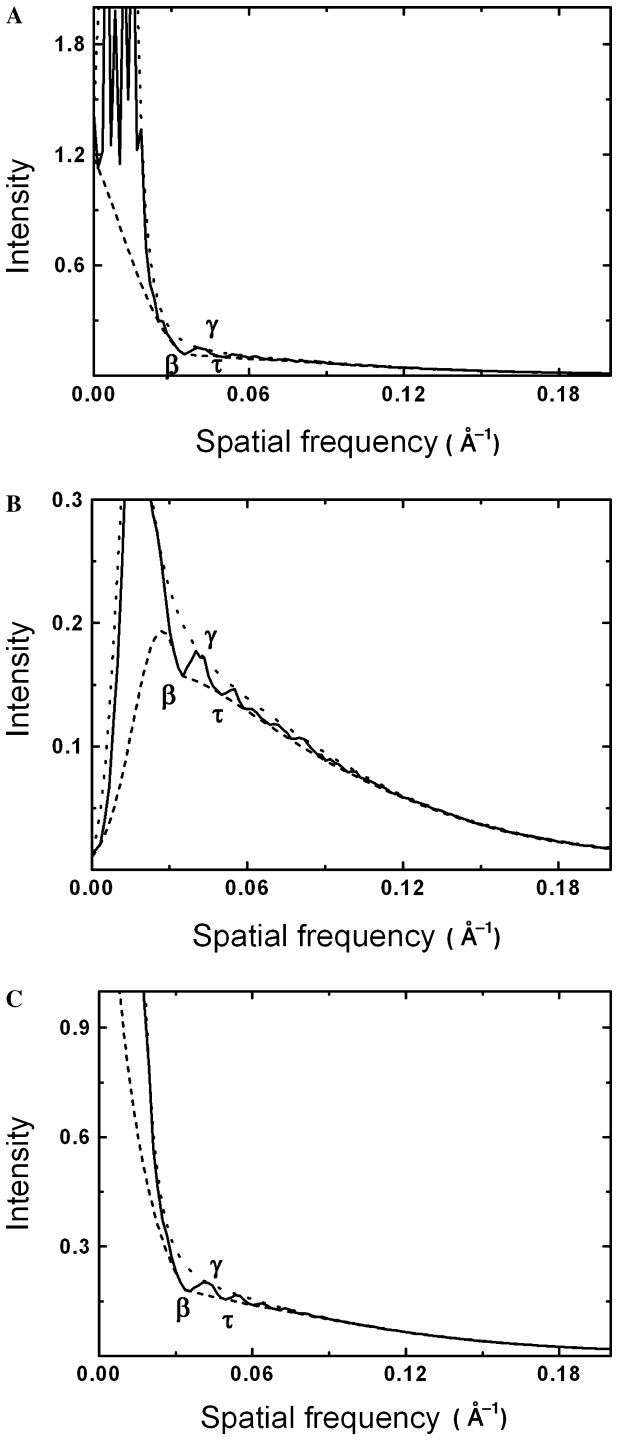

Fig. 6. The background (short dash line) and envelope (dotted line) are fitted to power spectra (solid line) calculated from the same KLH micrograph. The power spectra are based on: (A) windowed particles, (B) windowed sections of noise, and (C) overlapping sections of micrographs. The low-frequency behavior is very different in the three cases (see text).

method. Therefore, to evaluate the accuracy of our method we decided to rely on the concept of the self-consistency of the defocus settings of the set of micrographs, as outlined in (Mouche et al., 2001). The method

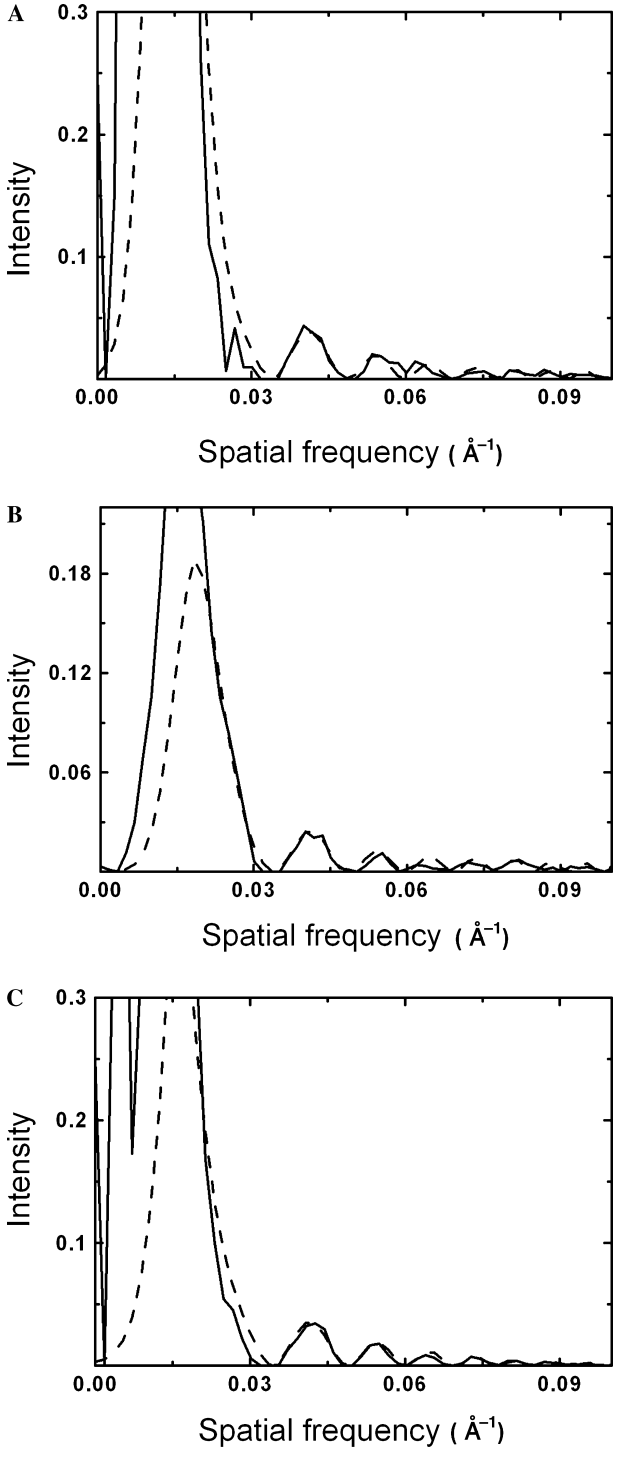

Fig. 7. The defocus determination on power spectra based on: (A) windowed particles, (B) windowed sections of noise, and (C) overlapping sections of micrographs for the same KLH micrograph (see Fig. 6). The defoci estimated automatically are 2.49, 2.51, and 2.47 μm, respectively, while the manually estimates for the defoci are 2.43, 2.50, and 2.48 μm, respectively. Although the low-frequency behavior of the original spectra (Fig. 6) is quite different, we arrive at quite consistent values of the defoci. This indicates that our procedure for eliminating the low-frequency region of power spectra from parameter determination is successful.

described in this work was designed for the purpose of correcting two of the CTF parameters (defocus and amplitude contrast) as a part of 3-D structure refinement procedure in single particle analysis. In this procedure the data, i.e., individual particle views, are grouped according to initially assigned defocus values. The initial assignment can be done using either manual CTF fitting or an automated procedure, such as the one proposed here. Next, the 3-D structures are calculated for each of the defocus groups using the current estimates of the orientation parameters and defocus values. Thus, each structure is affected by different CTF. Therefore, one can compare each of the structures with the structure that is obtained by merging (using Wiener filtration approach that involves CTF correction) the remaining structures. The comparison is done in Fourier space using the Fourier shell correlation technique (Saxton and Baumeister, 1982), which results in a 1-D cross-resolution curve. Due to the influence of the CTF, this curve should change sign in places corresponding to the zero-crossing of the CTF. Since it is easier to find locations of zero-crossings than minima of the attenuated curve (the power spectrum), the method is potentially more accurate.

For the tests we selected one of the data sets collected in our laboratory (Mullapudi et al., in preparation). The imaged specimen was 16S half proteasome prepared using spray method on Butvar film supported by a thin layer of carbon film with methylamine tungstate (MAT) as stain (Kolodziej et al., 1997). The images were recorded on a Jeol 1200 electron microscope at 100 kV and 50 k nominal magnification. 46 micrographs were selected for processing and digitized on a Zeiss-Imaging scanner (Z/I Imaging Corporation, Huntsville, AL) with a step size corresponding to a pixel size of 2.8 Å on the object scale. The power spectra were calculated using the Welch method of averaged periodograms with 50% overlap.

The defocus values were estimated three times: manually, using our automated procedure, and—after the structure was solved to approximately 13 Å resolution—using the procedure based on cross-resolution curves, as described above. In all cases the amplitude contrast was assumed to be constant and equal 0.1. The estimated defocus values were between approximately 7000 and 20 000 Å with one value of 25 700 Å. In order to compare three sets of estimates we calculated average errors defined as

$$E_{\Delta z} = \frac{1}{K}\sum_{k=1}^{K}\left|\Delta z_k^a - \Delta z_k^b\right|, \tag{29}$$

where superscripts indicate the CTF estimation method. The average error between the manual and the automated method was 170 Å, and the average errors between the defocus values obtained based on cross-resolution curves and manual and automated methods

were 270 and 338 Å, respectively. The respective maximum errors were 677, 820, and 1087 Å. The agreement between manual and automated estimates is excellent. In average, it is within the required accuracy. The relatively large maximum error is due to initial incorrect manual defocus estimation, which was discovered only after the automated analysis was performed. The larger errors with respect to the method based on cross-resolution curves are mainly due to the fact that this method generally yields lower defocus values than those obtained from an analysis of power spectra. This effect was observed earlier (Mouche et al., 2001)—the likely explanation is that the shape of cross-resolution curves is mainly due to the coherent signal from the aligned particle images, while the shape of power spectra is, in the case of processed data, mainly affected by the signal from the support carbon field. Thus, the respective sources of signal are located in different focal planes.

4.6. B-factor estimation, CF and PPF

Based on our analysis of the available material we conclude that a single *B*-factor cannot explain the behavior of the envelope (Fig. 8A). The red curve is a plot of the log(envelope) versus frequency squared. Clearly there is not a well-defined linear region, as there would be if the function were Gaussian. That is, there would seem to be at least two regions of the red curve that would seem to be linear and from which one might calculate *B*. This may also be seen in the attempt to match the CTF effect with the particle spectrum which lies in the lower part of the figure. It is clear that it would be impossible to match the black and blue curves throughout the entire frequency regime as illustrated in the graph. Based on the curves shown in Fig. 8A we conclude that the envelopes in cryo-EM are generally not Gaussian, and further speculate that the *B*-factor is an impoverished means to summarize micrograph quality, since there seems to be no relation between *B* and defocus, as demonstrated in Fig. 8B.

It was probably originally hoped that the *B*-factor would be enough to describe the tail of the power spectrum: that it should indicate both the attenuation of the signal and the frequencies where the predominant part of the power resides. We have separated these two concepts into two separate variables: CF and PPF. In Fig. 9A we show that CF yields a well-defined frequency above which we no longer expect to see reliable particle signal. Note that a cross-correlation coefficient of 0.8 selected in the context of Eq. (28) is a good cut-off criterion to find CF: the CTF oscillations (solid) no longer track the particle spectrum (dotted) above CF. In Fig. 9B we show that our definition of PPF yields good characterization of a micrograph information content. Different micrographs have PPF that vary greatly, and these PPF are not tightly correlated with the defoci, as shown in the figure: curves with defoci of 1.9, 3.1, 3.7, 4.7, and 5.3 μm, have PPF given by 0.130, 0.114, 0.140, 0.138, and 0.089 1/Å, respectively.

We tried to investigate how the three quantities, i.e., defocus, PPF and CF, might be related to one another. We took a series of 40S micrographs and plotted these quantities pair-wise in Figs. 10A–C and found no relation. We decided to follow a standard engineering practice and form unitless groupings among quantities and plot them: this is shown in Fig. 10D. Specifically, we plotted the product of CF and defocus versus the product of PPF and defocus. Empirically, the relationship is

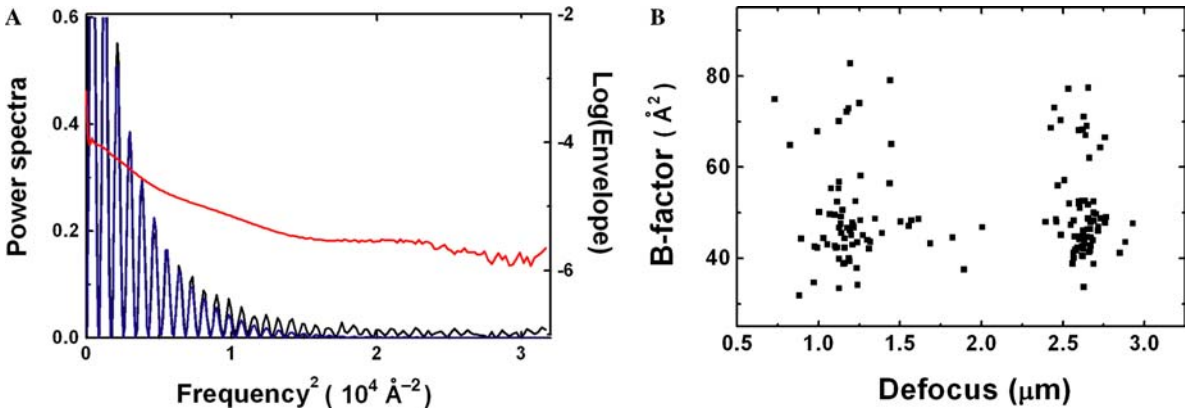

Fig. 8. *B*-factor is not a good characterization of micrographs: (A) The logarithm of the envelope (overall envelope minus background), which bounds the particle spectrum is shown as the red curve. Any attempt to fit a line segment to the red curve is doomed, meaning that a single *B*-factor cannot characterize the decay of the envelope. The black curve below represents the particle spectrum (power spectrum minus the background). The blue curve represents the CTF with parameters chosen such that the middle section of the curves fit well (frequencies below 0.01 Å^{-1}). Clearly one cannot fit this section of the curve (fit blue to black) and still have the curves match each other at higher frequencies. This is because the red curve does not maintain a linear shape: if the red curve were linear, one could fit the CTF curves to one another. (B) Another issue regarding *B*-factors is that there is no apparent relationship between *B*-factor and defocus (or any other quantity that might indicate micrograph quality). The analysis was done for KLH micrographs.

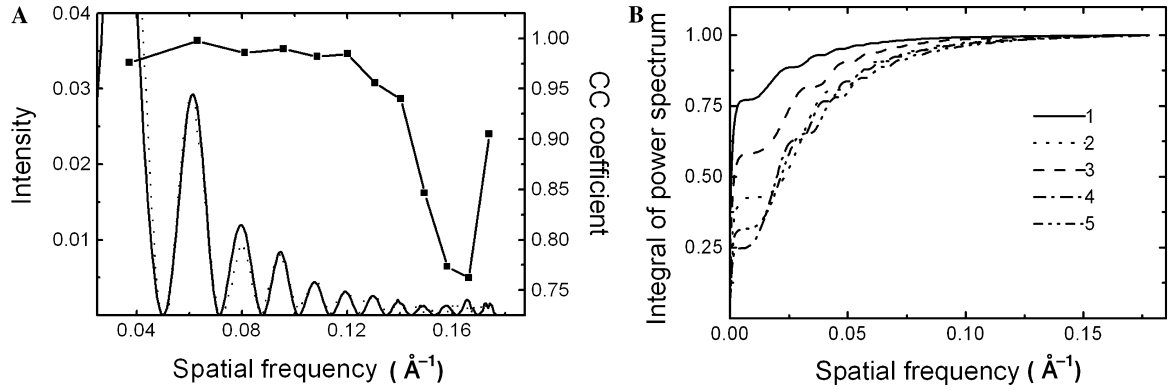

Fig. 9. Two characterizations of micrographs: cut-off frequency (CF) and principal power frequency (PPF). Without the simple *B*-factor to characterize decay, we introduce two natural frequencies related to the spectrum: (A) The spatial frequency at which we do not expect reliable data, we call the cut-off frequency (CF). This is the point at which the particle signal is no longer correlated to the CTF oscillations as the frequency is increased (see text). The criterion we use is that the cross-correlation Eq. (28) falls below 0.8. (B) Spatial frequency at which 99% of the integrated power resides. We call this predominant power frequency (PPF). Notice that the PPF is not correlated very closely to the defocus: for the curves numbered 2, 3, 5, 4, 1, we have defoci of 1.9, 3.1, 3.7, 4.7, and 5.3 μm, but PPF given by 0.130, 0.114, 0.140, 0.138, and 0.089 1/Å, respectively.

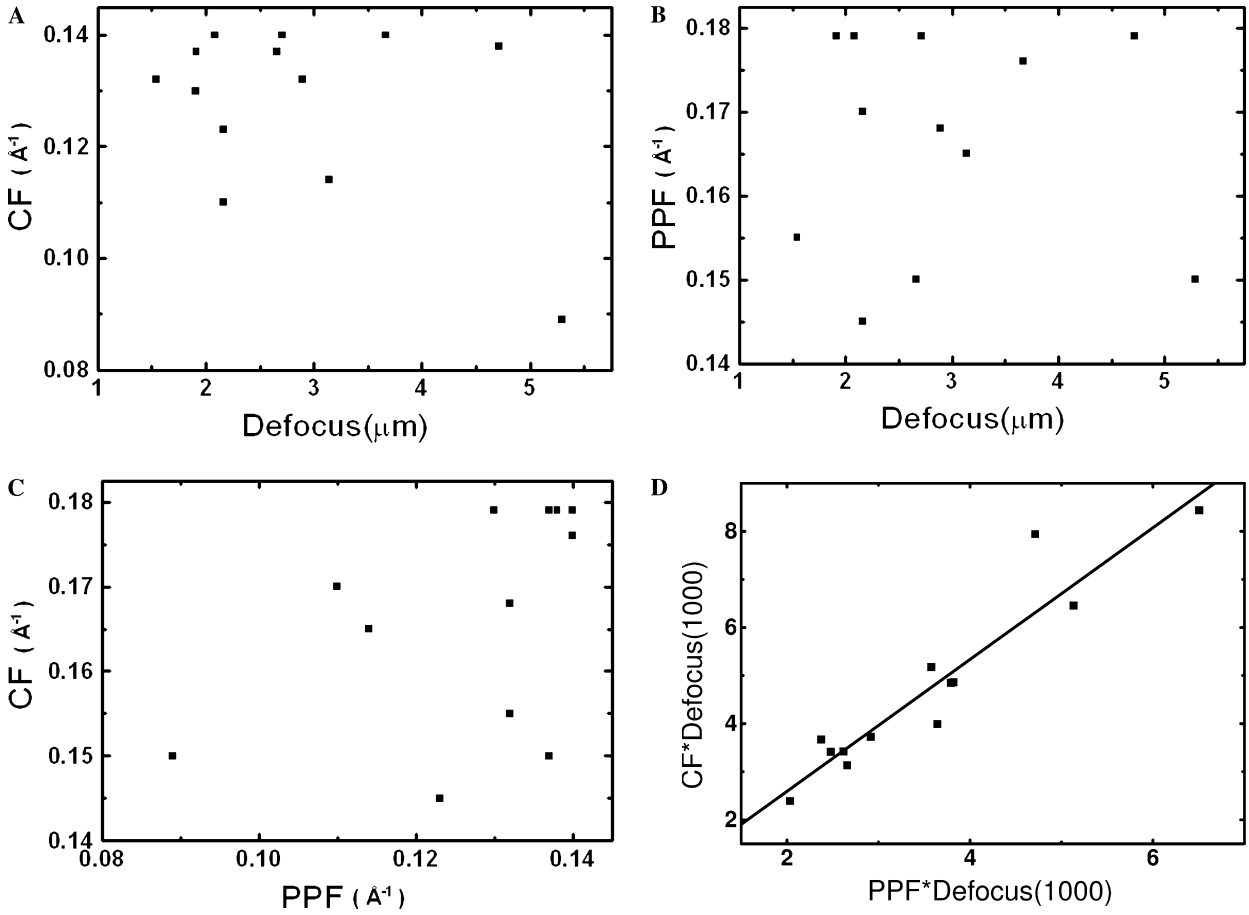

Fig. 10. There seems to be no strong relation between: (A) CF and defocus; (B) PPF and defocus; and (C) CF and PPF. One may form the two dimensionless groupings: product of PPF and defocus and a product of CF and defocus. When plotted, a nearly linear relation is seen to exit for 40S data: CF = 0.65PPF + 490/defocus.

nearly linear: CF = 0.65PPF + 490/defocus. Moreover since CF must be larger than PPF (recall that the frequencies higher than PPF still contain 1% of the spectrum), this suggests the following (not very stringent) bound: PPF<1300/defocus. We reflect on these relations in greater detail in the following discussion section.

5. Discussion

We have developed an effective inequality and equality constrained linear optimization based method to estimate the defocus and astigmatism of micrographs. We tested this method on far from focus and near to focus micrographs. The results agree well with manual estimations and with estimates based on cross-resolution curves. This method is successful in estimation of the envelope, the background noise, and defocus of micrographs with strong CTF effects, as well as micrographs with weak CTF effects. The method works on power spectra obtained for overlapping sections of micrographs, sections of noise, and for sections containing particles and it has been implemented in the SPIDER image processing system (Frank et al., 1996): http://www.wadsworth.org/spider_doc/spider/docs/spider_avail.html.

When the astigmatism is weak, it is relatively easy to find CTF zeros from the 1-D averaged power spectrum. Nevertheless, if there is a strong astigmatism, we need to use small angular sectors (3, even 2 degrees) to estimate directional defocus, because otherwise it is difficult to judge the position of the CTF zeros, and thereby determine the overall defocus. As for weak CTF cases, when the power spectrum may have only a single CTF peak, our automatic method even succeeds in distinguishing small differences between the parameters in two very similar, close to focus power spectra. Finally, we are able to obtain CTF parameters from both micrographs obtained for grids prepared with carbon support (where there is generally a strong CTF effect) and–equally successfully—without carbon support.

We estimated CTF parameters from power spectra obtained using three different strategies. Other researchers have already studied power spectra starting from overlapping sections of micrographs and small sections containing particles. We also used windowed sections of background noise, calculated the power spectra, and performed the analysis. The power spectra obtained for background noise have fewer peaks at low frequencies: this is advantageous for defocus estimation. On the other hand, power spectra obtained from windowed particles have large peaks at low frequency. Thus, when this strategy is used a sound method for accurate elimination of the low-frequency peaks should be employed. Moreover, since power spectra obtained using this strategy contain particle information that extends to middle and high frequencies, it is difficult to extract consistent CTF effects. Power spectra obtained using overlapping sections of micrographs were found to strike a useful balance, as the large degree of averaging results in smooth but accurate power spectra. As illustrated, such robust estimates simplify automated calculation of CTF parameters.

In order to perform our analysis, we needed to eliminate the very low-frequency sections of power spectra of micrographs, since these sections are not useful in determination of parameters. The fits of the background and envelope curves were performed only using a section beginning from the putative first theoretical CTF peak. We found that it was difficult to associate a *B*-factor with each micrograph, since the behavior of the appropriate envelope seemed to be piecewise Gaussian with quite different decays within respective parts of the power spectrum. Moreover, we determined that there was no relation between defocus and *B*-factor, contrary to the report (Saad et al., 2001; Sander et al., 2003). Instead of a single *B*-factor, we proposed two well-defined characteristics of the power spectrum: the CF, which is defined as the frequency where reliable signal can be detected, and PPF, which is defined as the frequency region where most of the integrated power resides. There seems to be no obvious relation between any two of the three quantities, CF, PPF and defocus. Instead, as we determined, there is a linear relation between CF, PPF and the inverse of the defocus. We may note that if we could keep the PPF fixed, moving closer to focus would increase the CF, which is in line with intuition. All other things being the same, moving closer to focus increases the frequency at which there is perceptible information content

It is a profound observation that we can vary microscope settings that result in uncorrelated changes in PPF and CF. This would indicate that the CF might take on the value of a frequency where the signal-to-noise ratio were arbitrarily small. One of the great challenges of cryo-microscopy is how to develop a method that would use high-frequency information content to align data, even if the integrated power in this frequency region might be small. The difficulty is that—as it currently stands—alignment procedures are designed such that they try to ensure that the predominant part of the power spectrum is reproduced. Therefore, the grand challenge for the design of the next generation of alignment algorithms is to solve structures that are not only correct to resolutions where the bulk of the signal resides (indicated by PPF) but to resolutions where there is reliable, albeit small, information content (indicated by CF).

Acknowledgments

We thank Joachim Frank for making 70S and 40S data sets available and Steven Ludtke for the GroEl data set. The KLH data set used in the work presented here was provided by the National Resource for Automated Molecular Microscopy, which is supported by the National Institutes of Health though the National Center for Research Resources' P41 program (RR17573). We thank Christian M.T. Spahn for helpful discussions. This work was supported by the NIH Grants R01 GM 60635

and P01 GM 064692, and The Welch Foundation Grant AU-1522 (to P.A.P.).

References

Barrodale, I., Roberts, F.D.K., 1978. An efficient algorithm for discrete L1 linear approximation with linear constraints. SIAM J. Numer. Anal. 15, 603–611.

Barrodale, I., Roberts, F.D.K., 1980. Solution of the constrained L1 linear approximation problem. ACM Trans. Math. Software 6, 231–235.

Bixby, R.E., 2002. Solving real-world linear programs: a decade and more of progress. Operat. Res. 50, 3–15.

Chong, E.K.P., Zak, S.H., 1996. An Introduction to Optimization. Wiley, New York.

Downing, K.H., Grano, D.A., 1982. Analysis of photographic emulsions for electron microscopy of two-dimensional crystalline specimens. Ultramicroscopy 7, 381–404.

Drenth, J., 1999. Principles of Protein X-ray Crystallography. Springer Verlag, New York.

Fernandez, J.-J., Sanjurjo, J.R., Carazo, J.M., 1997. A spectral estimation approach to contrast transfer function detection in electron microscopy. Ultramicroscopy 68, 267–295.

Frank, J., 1973. The envelope function of electron microscopic transfer function for partially coherent illumination. Optik 38, 519–536.

Frank, J., Penczek, P., Agrawal, R.K., Grassucci, R.A., Heagle, A.B., 2000. Three-dimensional cryoelectron microscopy of ribosomes. Methods Enzymol. 317, 276–291.

Frank, J., Radermacher, M., Penczek, P., Zhu, J., Li, Y., Ladjadj, M., Leith, A., 1996. SPIDER and WEB: processing and visualization of images in 3D electron microscopy and related fields. J. Struct. Biol. 116, 190–199.

Glaeser, R.M., Downing, K.H., 1992. Assessment of resolution in biological electron crystallography. Ultramicroscopy 47, 256–265.

Kenney, J.M., Hantula, J., Fuller, S.D., Mindich, L., Ojala, P.M., Bamford, D.H., 1992. Bacteriophage phi 6 envelope elucidated by chemical cross-linking, immunodetection, and cryoelectron microscopy. Virology 190, 635–644.

Kolodziej, S.J., Penczek, P.A., Stoops, J.K., 1997. Utility of Butvar support film and methylamine tungstate stain in three-dimensional electron microscopy: agreement between stain and frozen-hydrated reconstructions. J. Struct. Biol. 120, 158–167.

Kumaresan, R., 1993. Spectral analysis. In: Mitra, S.K., Kaiser, J.F. (Eds.), Handbook for Digital Signal Processing. Wiley, New York, pp. 1143–1242.

Ludtke, S.J., Jakana, J., Song, J.L., Chuang, D.T., Chiu, W., 2001. A 11.5 Å single particle reconstruction of GroEL using EMAN. J. Mol. Biol. 314, 253–262.

Malhotra, A., Penczek, P., Agrawal, R.K., Gabashvili, I.S., Grassucci, R.A., Junemann, R., Burkhardt, N., Nierhaus, K.H., Frank, J., 1998. *Escherichia coli* 70S ribosome at 15 Å resolution by cryo-electron microscopy: localization of fMet-tRNAfMet and fitting of L1 protein. J. Mol. Biol. 280, 103–116.

Mindell, J.A., Grigorieff, N., 2003. Accurate determination of local defocus and specimen tilt in electron microscopy. J. Struct. Biol. 142, 334–347.

Mouche, F., Boisset, N., Penczek, P.A., 2001. *Lumbricus terrestris* hemoglobin—The architecture of linker chains and structural variation of the central toroid. J. Struct. Biol. 133, 176–192.

Saad, A., Ludtke, S.J., Jakana, J., Rixon, F.J., Tsuruta, H., Chiu, W., 2001. Fourier amplitude decay of electron cryomicroscopic images of single particles and effects on structure determination. J. Struct. Biol. 133, 32–42.

Sander, B., Golas, M.M., Stark, H., 2003. Automatic CTF correction for single particles based upon multivariate statistical analysis of individual power spectra. J. Struct. Biol. 142, 392–401.

Saxton, W.O., Baumeister, W., 1982. The correlation averaging of a regularly arranged bacterial envelope protein. J. Microsc. 127, 127–138.

Spahn, C.M.T., Kieft, J.S., Grassucci, R.A., Penczek, P.A., Zhou, K.H., Doudna, J.A., Frank, J., 2001. Hepatitis C virus IRES RNA-induced changes in the conformation of the 40S ribosomal subunit. Science 291, 1959–1962.

Wade, R.H., 1992. A brief look at imaging and contrast transfer. Ultramicroscopy 46, 145–156.

Wade, R.H., Frank, J., 1977. Electron microscope transfer function for partially coherent axial illumination and chromatic defocus spread. Optik 49, 81–92.

Welch, P.D., 1967. The use of fast Fourier transform for the estimation of power spectra: A method based on time averaging over short modified periodograms. IEEE Trans. Audio Electroacoust. AU-15, 70–73.

Zhou, Z.H., Chiu, W., 1993. Prospects for using an IVEM with a FEG for imaging macromolecules towards atomic resolution. Ultramicroscopy 49, 407–416.

Zhu, J., Penczek, P.A., Schröder, R., Frank, J., 1997. Three-dimensional reconstruction with contrast transfer function correction from energy-filtered cryoelectron micrographs: procedure and application to the 70S *Escherichia coli* ribosome. J. Struct. Biol. 118, 197–219.

Zhu, Y., Carragher, B., Mouche, F., Potter, C.S., 2003. Automatic particle detection through efficient Hough transforms. IEEE Trans. Med. Imaging 22, 1053–1062.